García Segura, T.; Yepes Piqueras, V.; Alcalá González, J.; Pérez López, E. (2015). Hybrid harmony search for sustainable design of post-tensioned concrete box-girder pedestrian bridges. Engineering Structures. 92:112-122. doi:10.1016/j.engstruct.2015.03.015.

# HYBRID HARMONY SEARCH FOR SUSTAINABLE DESIGN OF POST-TENSIONED CONCRETE BOX-GIRDER PEDESTRIAN BRIDGES

Tatiana García-Segura[1]
Víctor Yepes[2]
Julián Alcalá[3]
Eloy Pérez-López[4]

## Abstract

This paper aims to find sustainable designs of post-tensioned concrete box-girder pedestrian bridges. A hybrid harmony search algorithm combining threshold optimization is used to find the geometry and the materials for which the sum of the costs or the emissions are the lowest, yet satisfying the requirements for structural safety and durability. An experimental design method was used to adjust the algorithm parameters. The parametric study was applied to three-span deck bridges ranging from 90 m to 130 m. The findings indicated that both objectives lead to similar cost results. However, the variables presented some differences. Such deviations suggested greater depths, more strands and a lower concrete strength for $CO_2$ target functions. Carbonation captured less than 1% of the deck emissions over 100 years. This methodology leads to a precise analysis of the practical rules to achieve an environmental design approach.

**Keywords**

Sustainable design; post-tensioned concrete; box-girder bridge; harmony search optimization.

[1] Graduate Research Assistant, Institute of Concrete Science and Technology (ICITECH), *Universitat Politècnica de València*, 46022 Valencia, Spain. E-mail: tagarse@cam.upv.es
[2] Associate Professor, Institute of Concrete Science and Technology (ICITECH), *Universitat Politècnica de València*, 46022 Valencia, Spain. **Corresponding author**. Phone +34963879563; Fax: +34963877569; E-mail: vyepesp@cst.upv.es
[3] Assistant Professor, Institute of Concrete Science and Technology (ICITECH), *Universitat Politècnica de València*, 46022 Valencia, Spain. E-mail: jualgon@cst.upv.es
[4] Project Co-ordinator, Offshore Renewable Energy Engineering Centre, SEEA, Cranfield University, MK43 0AL, Bedfordshire, United Kingdom. E-mail: epl@cranfield.ac.uk

## 1. Introduction

The construction industry has become one of the most carbon-intensive sectors [1]. Besides, construction requires large amounts of natural resources and therefore, resource depletion and damage to flora and fauna are unavoidable consequences. Concrete production emits large amounts of carbon dioxide, mainly due to high energy demands and limestone calcination during cement manufacture [2]. In 2007, clinker production reached around 55 million tons in Spain. This number dropped to 16.7 million tons in 2012 as a consequence of the financial crisis [3].

The World Commission on Environment and Development (WCED) reported on "Our Common Future", the long-term environmental strategies for achieving sustainable development [4]. The construction sector, an obstacle in advancing towards this goal, has sought new strategies for improving sustainability. Research activities have focused on comparing the emissions for different materials in construction activity [1,5,6], evaluating the life cycle emissions of concrete structures [2,7,8] and identifying optimal maintenance planning [9–11]. However, these approaches quantify the environmental effect once the design is completed. This study tackles the environmental challenge from the choice of the form and the materials involved in structural design.

Traditionally, technical guides and recommendations have provided a starting point for the design process. There are strict codes to assure an appropriate reliability and safety level. Concrete bridge loads and design codes has been developed by Fomento [12,13], the European Committee for Standardization (CEN) [14,15] and American Association of State Highway and Transportation Officials (AASHTO) [16]. Besides, several authors have provided guidance to achieve a proper box-girder bridge design [17,18]. The emergence of optimization methods to minimize the structural weight [19,20] and the economic cost [21–23] has enabled designers to explore new design forms. Both objectives lead to a reduction in material consumption and, therefore, their optimization is a good approach to achieve efficient designs. In this context, some authors have moved in this direction [24–27], proposing environmental emissions minimization. Similarly, the $CO_2$ emission as single-objective optimization is the focus in this research. Alternatively, Camp and Assadollahi [28] studied the $CO_2$ and cost optimization of RC footings as biobjectives by a multi-objective optimization method. They reported that more sustainable designs are less economical, while more economical designs are less sustainable.

This research differs from others in that it demonstrates the potential of a hybrid harmony search (HSTA) to find ecological and economic sustainable designs of continuous post-tensioned concrete box-girder pedestrian bridges. In addition, this study extends previous ones considering concrete carbonation as a negative emission. Carbonation during use stage decreases the total emissions by 22% [2]. If carbon capture is ignored, emission rates may be overestimated by as much as 13–48 % [7]. Carbonation rate depends on concrete strength and the geometry of the structure. Besides, the amount of carbonation will increase over time. This study evaluates carbonation during service life and checks whether the carbonation is notable for this structure. However, the calcium oxide that did not carbonate during the use stage can be carbonated after demolition [2].

Box-girder bridges have numerous advantages from the structural and constructive points of view, as the geometry is characterized by its strength to positive and negative bending moments and torsional stresses. Furthermore, the construction techniques can be cast in situ or precast in segments and then prestressed. Since several authors have advanced our understanding of the structural behavior [17, 18, 29–31] and codes present well-defined formulas to guarantee structural strength and serviceability [12–16], this paper presents a guide for designing more sustainable post-tensioned concrete box-girder pedestrian bridges.

To this end, a structural optimization tool was developed using a hybrid harmony search algorithm, which combines harmony search (HS) and threshold accepting (TA). Medeiros and Kripka used HS to optimize the monetary and environmental costs associated with pieces of rectangular reinforced concrete columns [32]. Kaveh and Shakouri Mahmud Abadi [33] improved HS by changing dynamically the pitch adjusting rate (PAR) with the generation number. They used the algorithm to optimize a composite floor system. Martí and González-Vidosa [34] proved the efficiency of TA for the pedestrian bridge optimization, although the SA appeared more efficient. A variant of TA improved the best results of reinforced concrete vaults in the study of Carbonell et al. [35]. Yepes et al. [27] proposed a hybrid multistart optimization strategic method based on a variable neighborhood search threshold acceptance strategy (VNS-MTAR) algorithm to design reinforced concrete cantilever retaining walls. Similarly, Martí et al. [36] employed the neighborhood structure of GA with the convergence properties of SA. In this line, Alia and Mandava [37] provided an overview of the variants of HS hybridization. This paper employs the hybridization strategy to combine the strengths of individual algorithms. The HS method is based on searching for perfect harmony by combining the musical notes of each instrument. It means finding the best dimensions of the box-girder, the concrete strength, the number of strands, the tendon layout and the reinforcing steel bars that together constitute a safe and sustainable pedestrian bridge. The economic cost and the $CO_2$ emissions are used as objective functions to compare the design alternatives. Carbonation is taken into account for emission evaluation as long as this process absorbs atmospheric carbon dioxide. This paper evaluates the importance of carbon capture.

## 2. Optimization problem definition

The problem proposed for this study involves a single-objective optimization of structural concrete. To this end, a program that determines the optimum values of the pedestrian bridge variables was created. This optimization aims to minimize the objective function associated with the cost (Eq. (1)) or the $CO_2$ emissions (Eq. (2)) while satisfying the constraints G represented by Eq. (3).

$$\mathrm{C}(\vec{x}) = \sum_{i=1,rc} p_i \cdot m_i(\vec{x}) \tag{1}$$

$$\mathrm{E}(\vec{x}) = \left(\sum_{i=1,re} e_i \cdot m_i(\vec{x})\right) - C_{CO_2}(\vec{x}) \tag{2}$$

$$G_j(\vec{x}) \le 0 \tag{3}$$

Note that the vector $x$ contains the discrete design variables. The values are discrete to adapt to real cases. The objective function is either the cost or the $CO_2$ emission. Optimization of one objective and evaluation of the other were undertaken simultaneously.

The total cost included the cost of materials for production, transport and placement. The cost during usage was not taken into account since the structure was designed to withstand the duration of its designed service life and, therefore, this study considered that there was no need for maintenance during this stage. The cost for the total number of construction units is given by Eq. (1), where $p_i$ are the unit prices and $m_i$ the measurements which depend on the design variables. The construction units associated with the cost (*rc*) are the volume of concrete, the amount of post-tensioned steel, the amount of reinforcement steel, the volume of lighting, the area of the formwork, the volume of scaffolding, and the $CO_2$ cost.

The unit prices and emissions (Table 1) were obtained from the 2013 BEDEC ITEC database of the Institute of Construction Technology of Catalonia [38]. Concrete unit price was determined for each compressive strength grade according to every component cost, including the cost of raw materials extraction, manufacture and transportation. This paper assumes a construction site in Valencia and distances were doubled after considering the return trip. The transport distances for cement, plasticizer, aggregate and silica fume were 32 km, 724 km, 12 km and 1420 km, respectively. Once the concrete was made, a mixer transported it from the concrete plant to the building site. This distance was considered as 40 km. The last construction unit is the cost of the $CO_2$ emissions given in SENDECO2 [39].

Likewise, the $CO_2$ emissions were assessed as defined in Eq. (2), where $e_i$ are the unit emissions. The construction units associated with the emissions (*rc*) are those of the cost, with the exception of the $CO_2$ cost. The plasticizer emission was obtained from the European Federation of Concrete Admixtures Associations [40] and the silica fume was considered not to have unit emissions since it is a waste product. During use stage, concrete carbonation absorbs $CO_2$ and, therefore, this capture ($C_{CO2}$) was deducted from the emissions (see Eq. (2)). The amount of $CO_2$ captured was estimated according to Eq. (4) [2, 41] based on the predictive models of Fick's First Law of Diffusion [42].

$$C_{CO_2}(\vec{x}) = k(\vec{x}) \cdot \sqrt{t(\vec{x})} \cdot c(\vec{x}) \cdot CaO \cdot r \cdot A(\vec{x}) \cdot M \qquad (4)$$

where $k$ is the carbonation rate coefficient (Table 2), $t$ is the structure service life (100 years), $c$ is the quantity of Portland cement per cubic meter of concrete (Table 2), $CaO$ is the amount of CaO content in

Portland cement (assumed to be 0.65), $r$ is the proportion of calcium oxide that can be carbonated (assumed to be 0.75), $A$ is the exposed surface area of the concrete, and $M$ is the chemical molar fraction ($CO_2$/CaO is 0.79). For durability conditions, this study considers that occluded air is less than 4.5%, and the box-girder surfaces, with the exception of the bottom slab, are exposed to rain. This leads to the carbonation rate coefficients given in Table 2. As Eq. (4) shows, the carbonation varies as the square of time. The carbonation is considered finalized when the service life ends. Note that maintenance activities are not included. The durability conditions guarantees a service life of 100 years.

## 2.1 Design variables

The parameters and design variables are, respectively, all the constant and variable data required to define the structural solution. The structural object of this work is a pedestrian three-span box-girder bridge, which is designed as a continuous beam deck with a box-girder cross section. Table 3 summarizes the parameters which are considered fixed for the structural solution. This study examines five deck lengths ranging from 90 m to 130 m. The deck is divided into three spans with a ratio of 0.8 between the spans. The pedestrian bridge width is 3.5 m. The construction is carried out with traditional scaffolding since the bridge height is 5 m.

Figure 1 shows the box-girder geometry and the reinforcement and Figure 2 illustrates the post-tensioned steel. The concrete is post-tensioned with strands symmetrically distributed through the webs. The parabolic layout is defined by the eccentricity in the sections where the bending moment is the minimum (supports) or the maximum (midspan for the central span and $0.375 \cdot L_2$ from the abutments). At these places, the eccentricity is the maximum, while, with respect to the distance between the center of the duct and the reinforcing bars, it is 1.5 times the duct diameter [13]. At the abutments, the tendons go through the cross section center. As post-tensioned steel variables, this study proposes the distance from the piers to the point of inflection ($L_{PI}$) and the number of strands ($N_S$). Each strand is prestressed to 195.52 KN.

The cross-section geometry is defined by seven variables: the depth ($h$), the width of the bottom slab ($b$), the width of the web inclination ($d$), the thickness of the top slab ($es$), the thickness of the external cantilever section ($ev$), the thickness of the bottom slab ($ei$) and the thickness of the webs ($ea$). The haunch length $(t)$ is conditioned by Schlaich and Scheff's [18] recommendations (see Eq. (5)).

Besides, the haunch must be large enough to guarantee that the ducts fit horizontally onto the high and low locations.

$$t = max\left\{\frac{b-2*ea}{5}, ei\right\} \quad (5)$$

Regarding the material, one variable is identified as the concrete strength (*fck*), ranging from 35 MPa to 100 MPa. The longitudinal reinforcing steel is defined by the number of bars per meter ($LR_{n1}$, $LR_{n2}$, $LR_{n3}$, $LR_{n4}$, $LR_{n5}$, $LR_{n6}$) and the diameter ($LR_{Ø1}$, $LR_{Ø2}$, $LR_{Ø3}$, $LR_{Ø4}$, $LR_{Ø5}$, $LR_{Ø6}$, $LR_{Ø7}$, $LR_{Ø8}$, $LR_{Ø9}$). The extra reinforcement covers the minimum bending moment (L/5 on both sides of the piers) at the top slab ($LR_{n1}$, $LR_{Ø7}$) and the maximum bending moment for the rest of the external ($LR_{n5}$, $LR_{Ø8}$) and central spans ($LRn_5$, $LR_{Ø9}$). The feasible set for the diameter variable includes 10, 12, 16, 20, 25 and 32 mm. Moreover, the extra reinforcement can be 0. Transverse reinforcement is determined by the diameter ($TR_{Ø1}$, $TR_{Ø2}$, $TR_{Ø3}$, $TR_{Ø4}$, $TR_{Ø5}$, $TR_{Ø6}$, $TR_{Ø7}$) and the spacing ($TR_S$).

## 2.2 Structural analysis

The deck was analyzed as a linear element with ten bars per span, and separately, the transverse analysis was modelled by a frame model. The structural model takes into account shear deformation and the effective flange width [43]. This modulus evaluates the stress envelopes due to a uniform load of 5 kN/m$^2$ and the deck self-weight including the bridge railing and asphalt (see Table 3). Besides, a 10 KN vertical load is applied over a 0.1 x 0.1 area for the local effects assessment [12]. Note that the thermal gradient [12], the prestressing steel effect and the differential settling in each support are also taken into account.

After that, the structural integrity analysis evaluates the limit states [12, 13]. Table 4 summarizes the ultimate and serviceability limit states. The ultimate limit state (ULS) assesses the capacity of flexure, shear, torsion, and torsion combined with flexure and shear. Besides, the minimum amount of reinforcement for the stress requirements and the geometrical conditions are also examined. The code on the actions for the design of road bridges [12] and the code on structural concrete [13] provide the equations to evaluate the structural capacity. The cracking serviceability limit state (SLS) requires compliance of the compression and tension cracks, as well as the decompression limit state in the area where the post-tensioned steel is located. The vibration limit state is checked according to the restrictions for concrete pedestrian bridges [13]. Regarding deflection, the instantaneous and time-dependent deflection was limited to 1/500th of the main span length for the characteristic combination [13], and the frequent value for the live loads is limited to 1/1200th of the main span length [12].

## 2.3 Constraints

This modulus verifies the demands of the safety, as well as those relating to the aptitude for service requirement. Note that this study does not consider penalty functions. Therefore, the limit states and the geometrical and constructability requirements must be guaranteed. The ULS checks whether the ultimate resistance is greater than the ultimate load effect (see Eq. (6)). For instance, the ULS of flexure calculates the ultimate iteration diagram $N_u$–$M_u$ and then checks whether the acting bending resultant is in the diagram.

$$R_u \geq S_u \tag{6}$$

where $R_u$ is the ultimate resistance of the structural response and $S_u$ is the ultimate load effect of actions.

The SLS covers all limit states for the required functionality, comfort or aspect requirements (see Eq. (7)).

$$C_s \geq E_s \tag{7}$$

where $C_s$ is the permitted value of serviceability limit state (cracking width, stresses, vibrations and deflection) and $E_s$ is the design value of the effect of actions.

## 2.4 Hybrid harmony search algorithm with threshold accepting

The heuristic method proposed for this study is a hybrid harmony search that simulates a musical harmony searching procedure. Harmony search was suggested by Geem et al. [44] based on jazz improvisation. The musicians play new combinations of notes from the outcomes of previous attempts. Memory and improvisation combining the notes (values) of each instrument (variables) leads to the best harmony (global optimum). HSTA combines HS with threshold accepting TA. TA was originally proposed by Dueck and Scheuer [45].

A flowchart for the HSTA algorithm is given in Figure 3. The procedure is described as follows:

Step 1 – Identification of the algorithm parameters. This algorithm requires the definition of the harmony memory size (HMS), the harmony memory considering rate (HMCR), the harmony memory probability (HMP), the pitch adjusting rate (PAR), the maximum number of improvisations without improvement (IWI) and the threshold iterations (TI).

Step 2 – Initialization of the harmony memory (HM). An HM matrix is generated with a total of HMS solution vectors. The values are randomly chosen from the permissible set. Then, the objective function is evaluated for each vector. Only feasible solutions are saved.

Step 3 – Improvisation of a new solution. Each value of the new solution is selected from the HM with a probability of HMCR, otherwise the new value is assigned randomly from the permissible set. For the first case, the value is selected from a solution vector according to its probability (Eq. (8)):

$$p(j) = \frac{\mathrm{HMP}^{j-1} * (1 - HMP)}{1 - HMP^{HMS}} \quad (8)$$

where $j$ is the position of the solution vector in the ranking. The first position corresponds to the best solution in the HM. This equation was proposed by Yepes and Medina [46] to build a population of solutions based on a greedy randomized adaptive search procedure. This approach provides an additional advantage to the best solutions depending on the parameter HMP. Calibrating this parameter we can adjust the population probability. Note that the sum of probabilities is equal to 1 and the extreme cases correspond to the deterministic choice (HMP=0) and the equal probability selection of the HMS solutions (HMP=1). Afterwards, this value is modified one position up or down if a new random number is smaller than the PAR rate. This process is repeated for the total number of variables ($m$).

Step 4 – Update the HM. The new solution replaces the worst harmony if its function value improves the worst one.

Step 5 – TA. After 200 iterations without improving the best harmony ($\mathrm{iter}_{\mathrm{IWITA}}$), a local search is carried out around this solution. Each iteration modifies up to 50% of the variables by one step. Threshold accepting accepts worse solutions when the increment is lower than a threshold value ($\Delta T$). Initially, a 5% increment in the function value is accepted. This threshold value is reduced gradually to zero during half of the TI. After that, only better solutions are accepted. This local search finishes when the number of TI is reached. The vector solution is updated in the HM if there is an improvement. Then, the procedure continues from Step 3.

Step 6 – Termination criterion. The algorithm ends when the number of sequential improvisations without improvement ($\mathrm{iter}_{\mathrm{IWI}}$) reaches the maximum IWI parameter.

Further, computer runs were performed nine times according to the methodology proposed by Payá-Zarforteza et al. [47] based on the extreme value theory.

## 3. Results from optimization procedures

An experimental design method was used to adjust the HSTA parameters. Instead of adjusting the optimum combination by a trial and error process, a statistical tool, MINITAB, studies the effect of each variable to find the best values. Table 5 shows the minimum and maximum values of a chosen range for

each parameter. The two-level experimental design studying five factors leads to a 32-case design. A half faction design was used to reduce the number of cases to 16. Each case was executed five times. The response surface model recommended the values illustrated in Table 5. Finally, the IWI was adjusted by stopping the procedure when the convergence criterion was achieved. This criterion recommended an IWI value of 1000.The proposed HSTA algorithm is compared with the conventional HS. Figure 4 shows the $CO_2$ emissions results for a 130 m deck length. HSTA improved the quality of solution in terms of $CO_2$ emissions about 8%, compared to HS.

## 4. Parametric study

This section compares the best designs for cost and $CO_2$ emission minimization for five deck lengths, ranging from 90 to 130 m. Analyzing the characteristics of the designs and identifying the differences between the criteria led to the definition of design rules for improving the sustainability of pedestrian bridges with box-girder cross sections. Note that the suggestions are limited to the range studied. Likewise, the geometrical restrictions hinder large differences between criteria.

Emission optimization compared to cost function, on average, reduces the emissions by 1% while increasing the cost by 2%. Figures 5 and 6 show the parabolic and linear relation between the deck length ($L$) and both the minimum cost per square meter of deck (C) and the minimum emission per square meter of deck (E), respectively. The differences in R-squared are less than 5%. Therefore, for the sake of simplicity, we consider the linear relations in the subsequent practical applications. Increasing the deck by one meter increases the price by 2.36 €/$m^2$ of deck, whether for the cost objective or the emission objective. From an environmental point of view, one meter of deck length increases the emissions by 5.49 kg $CO_2$/$m^2$ of deck and 4.96 kg $CO_2$/$m^2$ of deck for cost optimization and emission optimization, respectively. Therefore, as the length increases, the difference in $CO_2$ emissions between optimizing the cost and the emissions also increases. Even so, it is worth noting the little variation between both objectives. The carbon capture (CC) reduces the emissions between 1040 and 1436 kg $CO_2$ for the emission objective and between 942 and 1327 kg $CO_2$ for the cost objective (Figure 7). This represents less than 1% of the emissions. Hence, this geometry and the service life do not lead to large quantities of CC. To gain capture, the concrete should be crushed and reused after demolition.

Though criteria results indicated that emissions and cost optimization are closely related, the findings suggested some differences in the variables. The $CO_2$ target function found better solutions with

greater depth, more strands and lower concrete strength. The interpretation for this is similar to the one obtained by García-Segura et al. [41, 48] and Yepes et al. [24]. High-strength concrete uses greater amounts of cement and this material has a carbon-intensive production. On the other hand, the higher the exposed surface area, the greater the $CO_2$ capture.

Figure 8 illustrates the relationship between the depth ($h$) and the main span length ($L_1$). The ratio $h/L_1$ varied between 1/35 and 1/38 from an economic point of view and between 1/35 and 1/36 from an ecological point of view. Figure 9 shows the advisability of increasing the concrete strength ($f_{ck}$) in longer spans. The number of strands (Figure 10) can be represented by a linear function for the cost objective ($N_s$ = 1.0178$L$ - 60.978 with $R^2$= 0.9847) and the emission objective ($N_s$ = 0.9622$L$ – 51.089 with $R^2$= 0.9773).

The cantilever length ($v$) and the width of the bottom slab tended to be the maximum (1.05m) and the minimum (1.40m), respectively, to reduce the weight. However, some cases show smaller cantilevers and inclined webs due to the fact that decreasing the cantilever also decreases the longitudinal shear. The thickness of the top slab ($e_s$) and the external cantilever section ($e_v$) were 15 cm in all cases. So, the cantilever thickness was constant and the minimum proposed. The thickness of the bottom slab ($e_i$) was, on average, 16 cm and 19 cm for the best cost and emission solutions, respectively. Regarding the web, the thickness was greater for the cost-optimized (43 cm on average) and the emission-optimized (45 cm on average) solutions to hold the strands and guarantee the structural and constructability requirements. The haunch length ($t$) was determined by the thickness of the bottom slab and the number and dimensions of the ducts. Therefore, as the number of strands increased, so did the dimensions of $t$. The distance from the point of inflection to the pier ($L_{PI}$) was reduced as the span length increased to intensify the prestressing steel effect in the piers.

The following explains, in detail, the basic measurements to define the optimum design. Figure 11 illustrates the relationship between the volume of concrete (Co) and the deck length. As stated above, the environmental approach seeks a greater cross section and larger amounts of post-tensioned steel. Consequently, the volume of concrete and the amount of post-tensioned steel was, on average, 0.02m$^3$/m$^2$ of deck and 1.19kg/m$^2$ of deck greater for the emission objective. The linear relation between the amount of post-tensioned steel and the deck length (see Figure 12) shows that by increasing the deck length by one meter, the amount of post-tensioned steel per m$^2$ of deck increases by 0.321 kg/m$^2$ and 0.303 kg/m$^2$ for cost and emission optimization, respectively.

Figure 13 illustrates the amount of longitudinal reinforcing steel. Note that there was not a clear linear correlation with the deck length, but a good parabolic fit. Regarding the transverse reinforcement (see Figure 14), this was mainly influenced by the minimum reinforcing steel for slab bending. So, the greater the cross section, the higher the amount of transverse reinforcement required. In this context, the transverse reinforcement presented higher values for the emission objective.

## 5. Conclusions

A hybrid harmony search (HSTA) algorithm which combines TA optimization is proposed for optimizing the sustainability of post-tensioned concrete box-girder pedestrian bridges. The three-span deck bridge has a ratio of 0.8 between the spans. An experimental design method is used to find the best combination of algorithm parameters. The economic cost and the $CO_2$ emissions are selected as the objective functions based on production materials, transport and placement. Both objectives lead to a reduction in materials consumption, conditioned by the unit costs and emissions values. The findings indicate that the environmental goal also ensures economic solutions, since the results show 1% less pollution and 2% more expense. However, the analysis of the main characteristics reveals that the $CO_2$ objective function achieves better solutions with greater depths, more strands and lower concrete strength. Therefore, despite the small differences due to the geometrical restrictions, the trends show the way to achieve environmental benefits.

The costs and emissions per square meter of deck vary as a linear function of the deck length. Increasing the deck by one meter involves an increment of 2.36 €/$m^2$ of deck and 5.49 $kgCO_2/m^2$ of deck from an economic point of view, and 2.36 €/$m^2$ of deck and 4.96 $kgCO_2/m^2$ of deck from an ecological point of view. The relation between the depth and the main span length ranges from 1/35 and 1/38 for the minimum cost objective, and between 1/35 to 1/36 for the emission objective. Regarding concrete strength, it should be increased as long as the deck lengthens. CC during the 100 years of service life represents only 1% of the emissions. Therefore, this article shows that carbonation is not significant for this structure and only by means of concrete reuse it is possible to strengthen the $CO_2$ capture. The results of this study contribute to increasing the practical rules in designing pedestrian bridges. Besides, this paper opens up the range of variables by adding the possibility of using high-strength concrete.

**Acknowledgements**

This research was financially supported by the Spanish Ministry of Science and Innovation (Research Project BIA2011-23602).

**References**


[1] Liu S, Tao R, Tam CM. Optimizing cost and $CO_2$ emission for construction projects using particle swarm optimization. Habitat Int 2013; 37:155–162.

[2] García-Segura T, Yepes V, Alcalá J. Life cycle greenhouse gas emissions of blended cement concrete including carbonation and durability. Int J Life Cycle Assess 2014; 19(1):3–12.

[3] Oficemen. Annual report of Spanish cement sector 2012; 2012. Available at: www.oficemen.com/Uploads/docs/Anuario 2012%281%29.pdf. (September 1, 2014)

[4] United Nations. Report of the World Commission on Environment and Development: Our Common Future; 1987. Available at: www.are.admin.ch/themen/nachhaltig/00266/00540/00542/index.html?lang=en. (August 27, 2014)

[5] Börjesson P, Gustavsson L. Greenhouse gas balances in building construction: wood versus concrete from life-cycle and forest land-use perspectives. Energy Policy 2000; 28(9):575–588.

[6] González MJ, García Navarro J. Assessment of the decrease of $CO_2$ emissions in the construction field through the selection of materials: Practical case study of three houses of low environmental impact. Build Environ 2006; 41(7):902–909.

[7] Collins F. Inclusion of carbonation during the life cycle of built and recycled concrete: influence on their carbon footprint. Int J Life Cycle Assess 2010; 15(6):549–556.

[8] Tae S, Baek C, Shin S. Life cycle $CO_2$ evaluation on reinforced concrete structures with high-strength concrete. Environ Impact Assess Rev 2011; 31(3):253–260.

[9] Liu M, Frangopol DM. Optimal bridge maintenance planning based on probabilistic performance prediction. Eng Struct 2004; 26(7):991–1002.

[10] Yang S, Frangopol DM, Kawakami Y, Neves LC. The use of lifetime functions in the optimization of interventions on existing bridges considering maintenance and failure costs. Reliab Eng Syst Saf 2006; 91(6):698–705.

[11] Orcesi AD, Frangopol DM. Probability-based multiple-criteria optimization of bridge maintenance using monitoring and expected error in the decision process. Struct Multidiscip Optim 2011; 44(1):137–148.

[12] Fomento M. IAP-11: Code on the actions for the design of road bridges. Madrid, Spain: Ministerio de Fomento; 2011 [in Spanish].

[13] Fomento M. EHE-08: Code on structural concrete. Madrid, Spain: Ministerio de Fomento; 2008 [in Spanish].

[14] CEN. Eurocode 1: Actions on structures-Part 2: Traffic loads bridges. EB 1991-2:2003 (EC-1).

[15] CEN. Eurocode 2: Design of concrete structures- Part 2: Concrete Bridge-Design and detailing rules EN1992-2:2005 (EC-2).

[16] AASHTO. AASHTO LRFD Bridge Design Specifications 2012.AASHTO LRFD 2012.

[17] Schlaich J, Scheff H. Concrete Box-girder Bridges. International Association for Bridge and Structural Engineering. Zürich, Switzerland; 1982.

[18] Fomento M. New overpasses: general concepts. Madrid, Spain: Ministerio de Fomento; 2000 [in Spanish].

[19] Li LJ, Huang ZB, Liu F. A heuristic particle swarm optimization method for truss structures with discrete variables. Comput Struct 2009; 87(7–8):435–443.

[20] Felkner J, Chatzi E, Kotnik T. Interactive particle swarm optimization for the architectural design of truss structures. In: IEEE Symposium on Computational Intelligence for Engineering Solutions (CIES). Singapore; 2013:15-22.

[21] Martí JV, Yepes V, González-Vidosa F. A memetic algorithm approach to designing of precast-prestressed concrete road bridges with steel fiber-reinforcement. ASCE J Struct Eng ASCE 2015; 141(2):04014114.

[22] Madhkhan M, Kianpour A, Torki Harchegani ME. Life-cycle cost optimization of prestressed simple-span concrete bridges with simple and spliced girders. IJST, Trans Civ Eng 2013; 37:53–66.

[23] Martínez-Martín F.J, González-Vidosa F, Hospitaler A. Yepes V, A parametric study of optimum tall piers for railway bridge viaducts. Struct Eng Mech 2013; 45(6):723–740.

[24] Yepes V, Martí JV, García-Segura T, Cost and $CO_2$ emission optimization of precast-prestressed concrete U-beam road bridges by a hybrid glowworm swarm algorithm. Autom Constr 2015; 49:123-134.
[25] Paya-Zaforteza I, Yepes V, Hospitaler A. González-Vidosa F. $CO_2$-optimization of reinforced concrete frames by simulated annealing. Eng Struct 2009; 31(7):1501–1508.
[26] Camp CV, Huq F. $CO_2$ and cost optimization of reinforced concrete frames using a big bang-crunch algorithm. Eng Struct 2013; 48:363–372
[27] Yepes V, Gonzalez-Vidosa F, Alcala J, Villalba P. $CO_2$-optimization design of reinforced concrete retaining walls based on a VNS-threshold acceptance strategy. J Comput Civ Eng 2012; 26(3):378–386.
[28] Camp CV, Assadollahi A. $CO_2$ and cost optimization of reinforced concrete footings using a hybrid big bang-big crunch algorithm. Struct Multidisc Optim 2013; 48(2):411-426.
[29] Ates S. Numerical modelling of continuous concrete box girder bridges considering construction stages. Appl Math Model 2011; 35(8):3809–3820.
[30] Kurian B, Menon D. Correction of errors in simplified transverse bending analysis of concrete box-girder bridges. J Bridg Eng 2005; 10:650–657.
[31] Mentrasti L. Torsion of box girders with deformable cross sections. J Eng Mech 1991; 117(10):2179–2200.
[32] Medeiros GF, Kripka M. Optimization of reinforced concrete columns according to different environmental impact assessment parameters. Eng Struct 2014; 59:185–194.
[33] Kaveh A, Shakouri Mahmud Abadi A. Cost optimization of a composite floor system using an improved harmony search algorithm. J Constr Steel Res 2010; 66(5):664-669.
[34] Martí JV, González-Vidosa F. Design of prestressed concrete precast pedestrian bridges by heuristic optimization. Adv Eng Softw. 2010; 41(7–8):916–922
[35] Carbonell A, González-Vidosa F, Yepes V. Design of reinforced concrete road vaults by heuristic optimization. Adv Eng Softw 2011; 42(4):151–159.
[36] Martí JV, Gonzalez-Vidosa F, Yepes V, Alcalá J. Design of prestressed concrete precast road bridges with hybrid simulated annealing. Eng Struct 2013; 48:342–352.
[37] Alia OM, Mandava R. The variants of the harmony search algorithm: an overview. Artif Intell Rev 2011; 36(1):49–68
[38] Catalonia Institute of Construction Technology. BEDEC PR/PCT ITEC materials database. Barcelona, Spain. Available at: www.itec.cat. (August 10, 2014).
[39] Sende$CO_2$. Carbon dioxide emission allowances electronic trading system. Available at: www.sendeco2.com. (August 12, 2014)
[40] European Federation of Concrete Admixtures Associations. Environmental Product Declaration (EPD) for Normal Plasticising admixtures. 2006. Available at: www.efca.info/downloads/324%20ETG%20Plasticiser%20EPD.pdf. (August 10, 2014)
[41] García-Segura T, Yepes V, Martí JV, Alcalá J. Optimization of concrete I-beams using a new hybrid glowworm swarm algorithm. Lat Am J Solids Struct 2014; 11(7):1190–1205.
[42] Lagerblad B. Carbon dioxide uptake during concrete life cycle – State of the art. Swedish Cement and Concrete Research Institute; 2006:1-47.
[43] Fomento M. RPX-95: Recommendations for steel-concrete composite road bridges project. Madrid, Spain: Ministerio de Fomento; 1995 [in Spanish].
[44] Geem Z, Kim, JH. Loganathan GV. A new heuristic optimization algorithm: harmony search. Simulation 2001; 76(2):60–68.
[45] Dueck G, Scheuer T. Threshold accepting: A general purpose optimization algorithm appearing superior to simulated annealing. J Comput Phys 1990; 90(1):161–175.
[46] Yepes V, Medina JR. Economic heuristic optimization for heterogeneous fleet VRPHESTW. J Transp Eng 2006; 132(4):303-311.
[47] Payá-Zaforteza I, Yepes V, González-Vidosa F, Hospitaler A. On the Weibull cost estimation of building frames designed by simulated annealing. Meccanica 2010; 45(5):693-704.

[48] García-Segura T, Yepes V, Alcalá J. Sustainable design using multiobjective optimization of high-strength concrete I-beams. In: The 2014 International Conference on High Performance and Optimum Design of Structures and Materials HPSM/OPTI. Ostend, Belgium; 2014:347–358.

**Table 1** Basic prices and $CO_2$ emissions

| Unit measurements | Cost (€) | Emission ($kgCO_2$) |
|---|---|---|
| $m^3$ of scaffolding | 10.02 | 6.92 |
| $m^2$ of formwork | 33.81 | 2.08 |
| $m^3$ of lighting | 104.57 | 604.42 |
| kg of steel (B-500-S) | 1.16 | 3.03 |
| kg of active steel (Y1860-S7) | 3.40 | 5.64 |
| $m^3$ of concrete HP-35 | 104.57 | 321.92 |
| $m^3$ of concrete HP-40 | 109.33 | 338.90 |
| $m^3$ of concrete HP-45 | 114.10 | 355.88 |
| $m^3$ of concrete HP-50 | 118.87 | 372.86 |
| $m^3$ of concrete HP-55 | 123.64 | 389.84 |
| $m^3$ of concrete HP-60 | 128.41 | 406.82 |
| $m^3$ of concrete HP-70 | 137.95 | 440.78 |
| $m^3$ of concrete HP-80 | 147.49 | 474.74 |
| $m^3$ of concrete HP-90 | 157.02 | 508.70 |
| $m^3$ of concrete HP-100 | 166.56 | 542.66 |
| t $CO_2$ emission | 5.00 | |

**Table 2** Mix design properties and cement content

| Unit | ***k* exposed to rain ($mm/year^{0.5}$)** | ***k* protected from rain ($mm/year^{0.5}$)** | **Cement ($kg/m^3$)** |
|---|---|---|---|
| $m^3$ of concrete HP-35 | 1.50 | 3.01 | 300 |
| $m^3$ of concrete HP-40 | 1.25 | 2.50 | 320 |
| $m^3$ of concrete HP-45 | 1.05 | 2.11 | 350 |
| $m^3$ of concrete HP-50 | 0.90 | 1.81 | 400 |
| $m^3$ of concrete HP-55 | 0.79 | 1.57 | 457 |
| $m^3$ of concrete HP-60 | 0.69 | 1.38 | 485 |
| $m^3$ of concrete HP-70 | 0.55 | 1.09 | 493 |
| $m^3$ of concrete HP-80 | 0.45 | 0.89 | 497 |
| $m^3$ of concrete HP-90 | 0.37 | 0.74 | 517 |
| $m^3$ of concrete HP-100 | 0.31 | 0.63 | 545 |

**Table 3.** Main parameters of the analysis

| | |
|---|---|
| ***Geometrical parameters*** | |
| Pedestrian bridge width | A = 3.5 m |
| Number of spans | 3 |
| Deck length | L = 90 – 100 – 110 – 120 – 130 m |
| Central span length | $L_1$ = 34.6 – 38.40 – 42.4 – 46.2 – 50 m |
| External span length | $L_2$ = 27.7 – 30.8 – 33.8 – 36.9 - 40 m |
| Clearance | 5 m |
| Diaphragm thickness | 1.2 m |
| ***Material parameters*** | |
| Maximum aggregate size | 20 mm |
| Reinforcing steel | B-500-S |
| Post-tensioned steel | Y1860-S7 |
| Strand diameter | $\Phi_s$ = 0.6” |
| Tensioning time | 7 days |
| ***Loading related parameters*** | |
| Reinforced concrete self-weight | 25 KN/m$^3$ |
| Asphalt layer self-weight | 24 KN/m$^3$ |
| Bridge railing self-weight | 1 KN/m |
| Uniform load | 5 KN/m$^2$ |
| Point load | 10 KN |
| Differential settling | 5 mm |
| ***Exposure related parameters*** | |
| External ambient conditions | IIb |
| ***Code related parameters*** | |
| Code regulation | EHE-08/IAP-11 |
| Service working life | 100 years |

**Table 4.** Ultimate and serviceability limit states

| **Limit States** |
|---|
| - Vertical shear |
| - Longitudinal shear |
| - Punching shear |
| - Bending |
| - Torsion |
| - Torsion combined with bending and shear |
| - Crack width < 0.2 mm |
| - Compression and tension stress. Decompression in post-tensioned steel depth |
| - Vibration. First mode frequency $f_o$>5Hz or static deflection produced by a 75 kg pedestrian (ye) $ye \leq \frac{0.5*\sqrt{f_0}}{4*\pi^2*{f_0}^2*k*\psi}$, where k is 0.8 for 3 spans with a length relation of 0.8 and ψ is 8.7, 9.8 and 10.8 for a span length of 30 m, 40 m and 50 m, respectively. |
| - Deflection. Deflection for the characteristic combination <1/500*main span length. Deflection for the frequent value for the live loads<1/1200*main span length |

**Table 5.** Experimental design method

| | HMS | HMCR | HMP | PAR | TI |
|---|---|---|---|---|---|
| Minimum value | 50 | 0.7 | 0.6 | 0.1 | 200 |
| Maximum value | 200 | 1 | 0.9 | 0.4 | 1000 |
| Best value | 200 | 0.7 | 0.75 | 0.4 | 1000 |

**Table 6.** Mean geometrical variables of best cost (c) and best emission (e) optimized solutions for 90-100-110-120-130 m decks

| $L$ (m) | | $h$ (m) | $b$ (m) | $v$ (m) | $e_s$ (m) | $e_v$ (m) | $e_i$ (m) | $e_a$ (m) | $t$ (m) | $f_{ck}$ (MPa) | $L_{PI}$ | $N_s$ |
|---|---|---|---|---|---|---|---|---|---|---|---|---|
| 130 | (c) | 1.35 | 1.42 | 0.89 | 0.15 | 0.15 | 0.16 | 0.43 | 0.28 | 52.78 | 0.06 | 69.78 |
| | (e) | 1.39 | 1.41 | 1.05 | 0.15 | 0.15 | 0.19 | 0.43 | 0.27 | 48.89 | 0.05 | 73.78 |
| 120 | (c) | 1.22 | 1.42 | 1.02 | 0.16 | 0.15 | 0.17 | 0.43 | 0.27 | 47.78 | 0.09 | 64.44 |
| | (e) | 1.27 | 1.40 | 1.05 | 0.15 | 0.15 | 0.23 | 0.43 | 0.26 | 43.89 | 0.08 | 64.67 |
| 110 | (c) | 1.18 | 1.42 | 1.01 | 0.15 | 0.15 | 0.16 | 0.45 | 0.16 | 46.67 | 0.11 | 49.56 |
| | (e) | 1.18 | 1.40 | 1.05 | 0.15 | 0.15 | 0.21 | 0.47 | 0.21 | 41.11 | 0.09 | 56.67 |
| 100 | (c) | 1.08 | 1.43 | 1.00 | 0.15 | 0.15 | 0.15 | 0.44 | 0.15 | 40.00 | 0.14 | 40.00 |
| | (e) | 1.08 | 1.41 | 1.04 | 0.15 | 0.15 | 0.16 | 0.45 | 0.16 | 40.00 | 0.16 | 41.33 |
| 90 | (c) | 0.98 | 1.40 | 1.00 | 0.15 | 0.15 | 0.15 | 0.41 | 0.15 | 40.00 | 0.20 | 31.11 |
| | (e) | 0.98 | 1.41 | 1.04 | 0.15 | 0.15 | 0.17 | 0.49 | 0.17 | 36.67 | 0.17 | 37.33 |

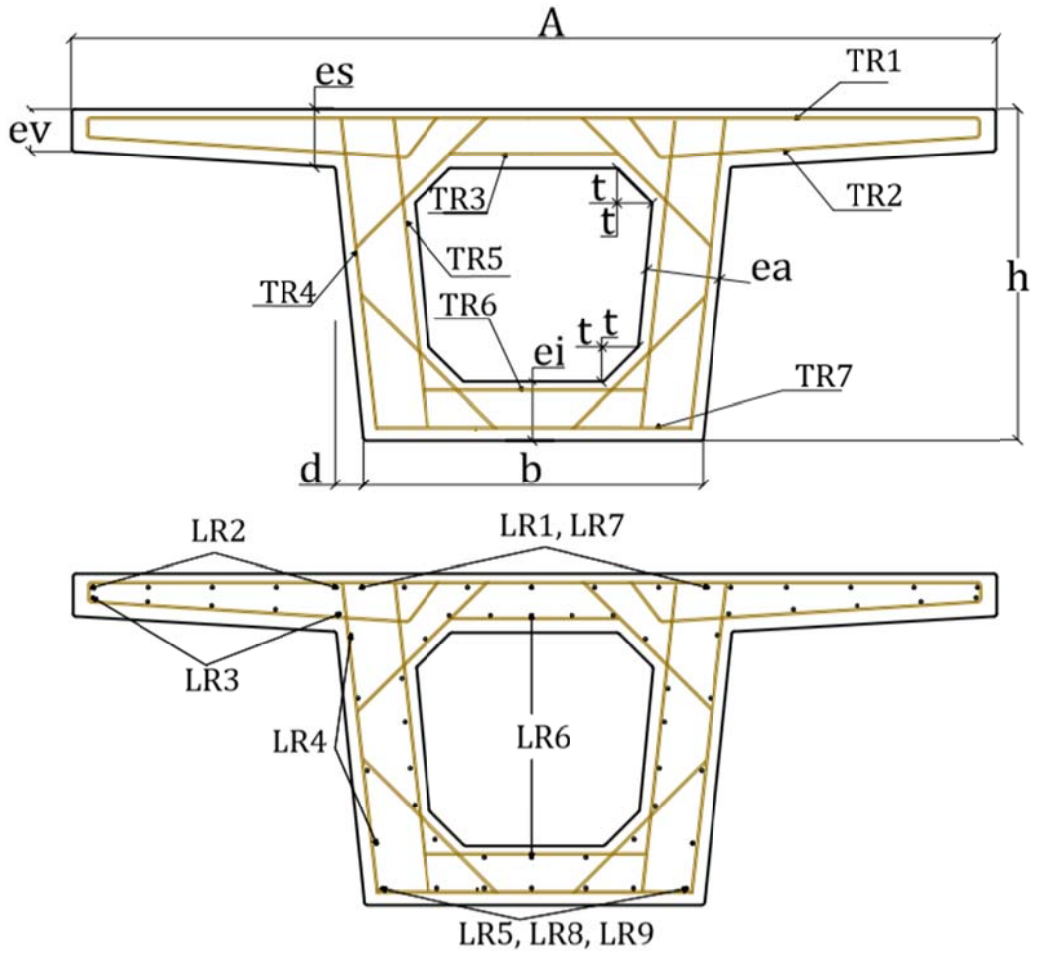


**Fig. 1.** Box-girder geometry and reinforcing steel

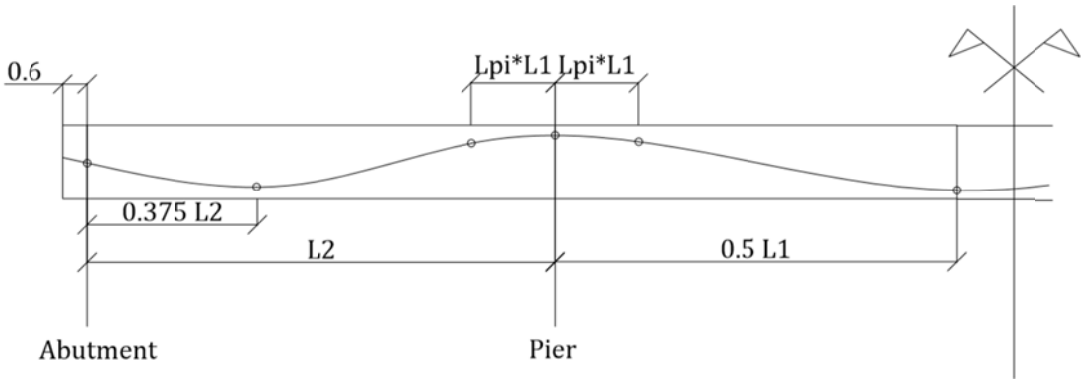


**Fig. 2**. Post-tensioned steel

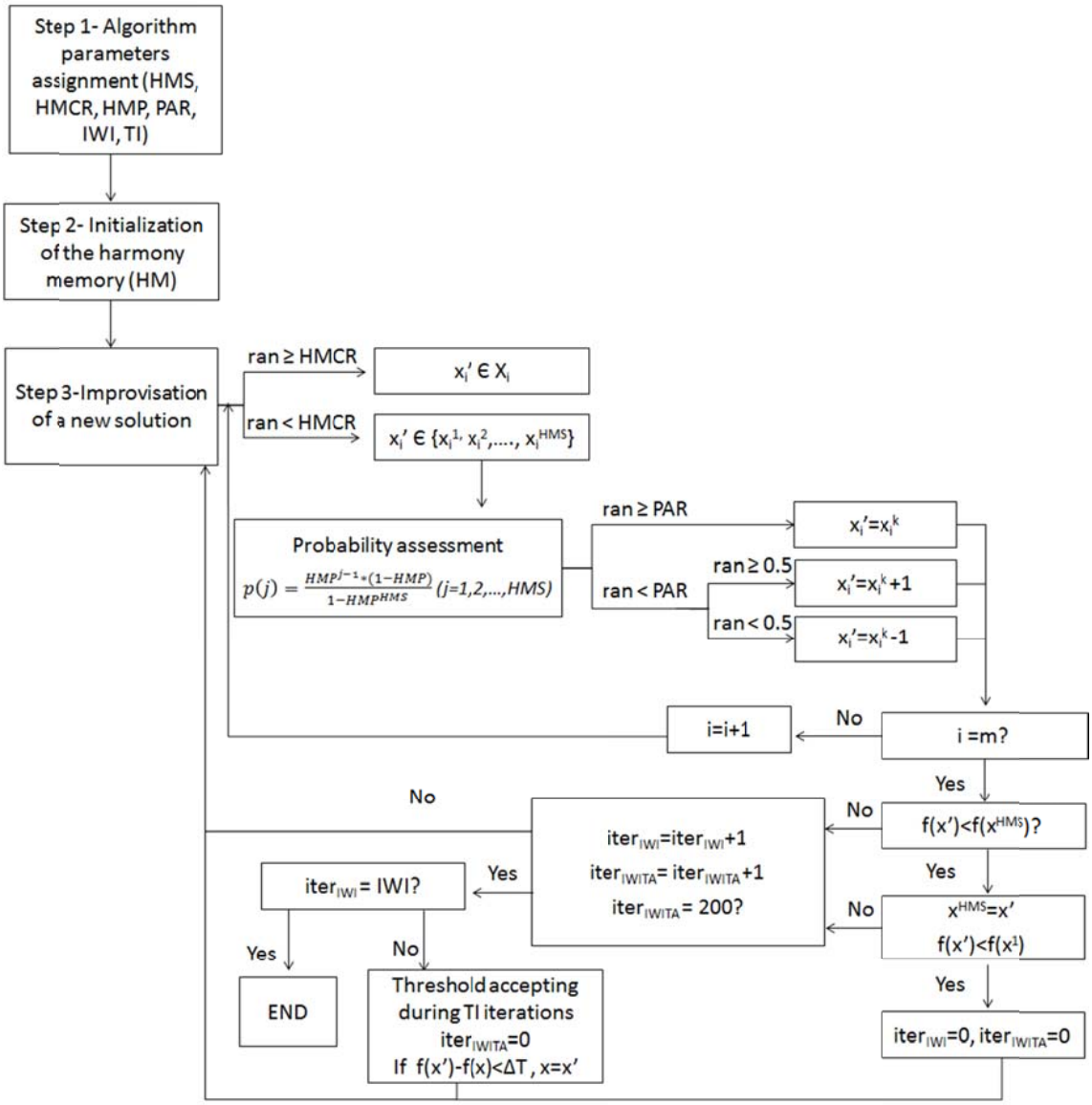


**Fig. 3.** HSTA flowchart

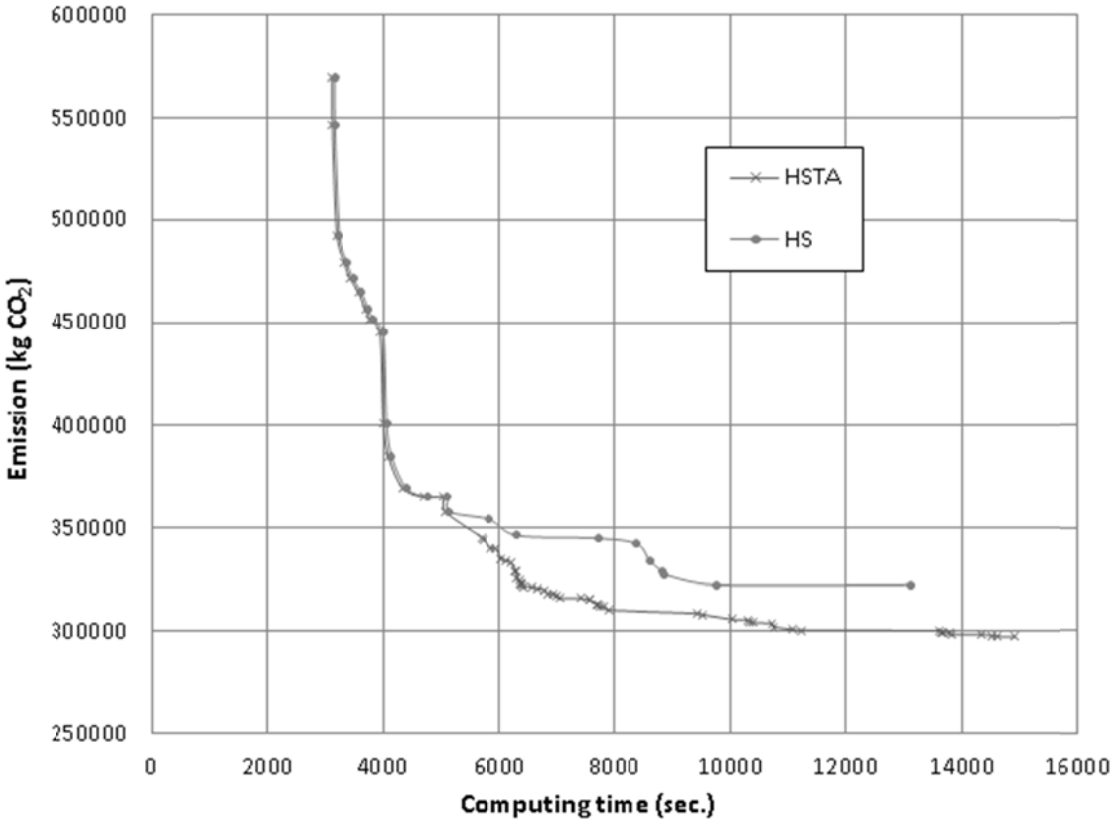


**Fig. 4.** Emissions and computing time for HSTA and HS algorithms

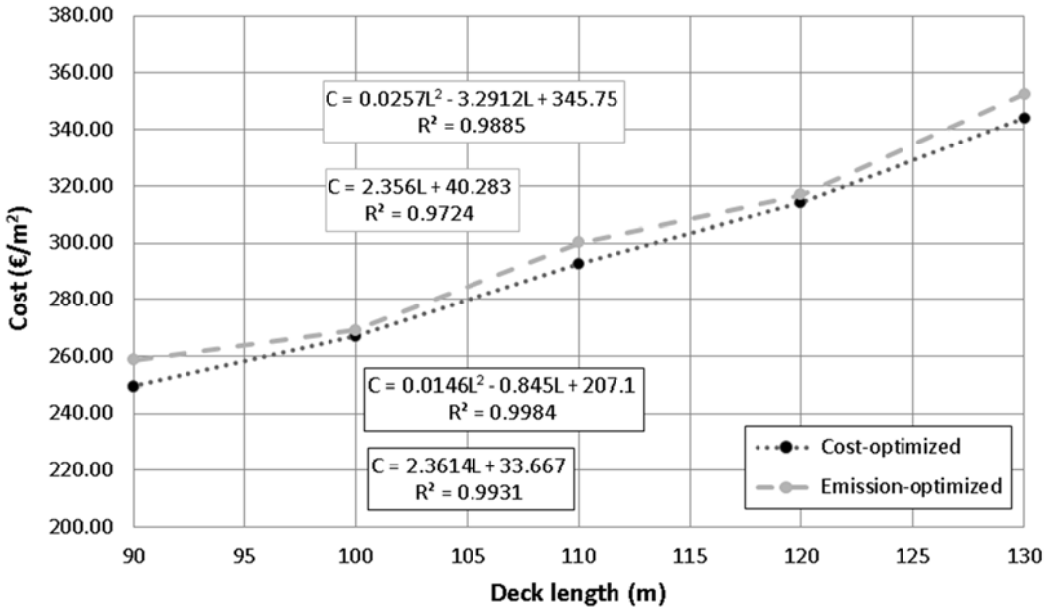


**Fig. 5.** Mean cost per $m^2$ of deck according to the deck length

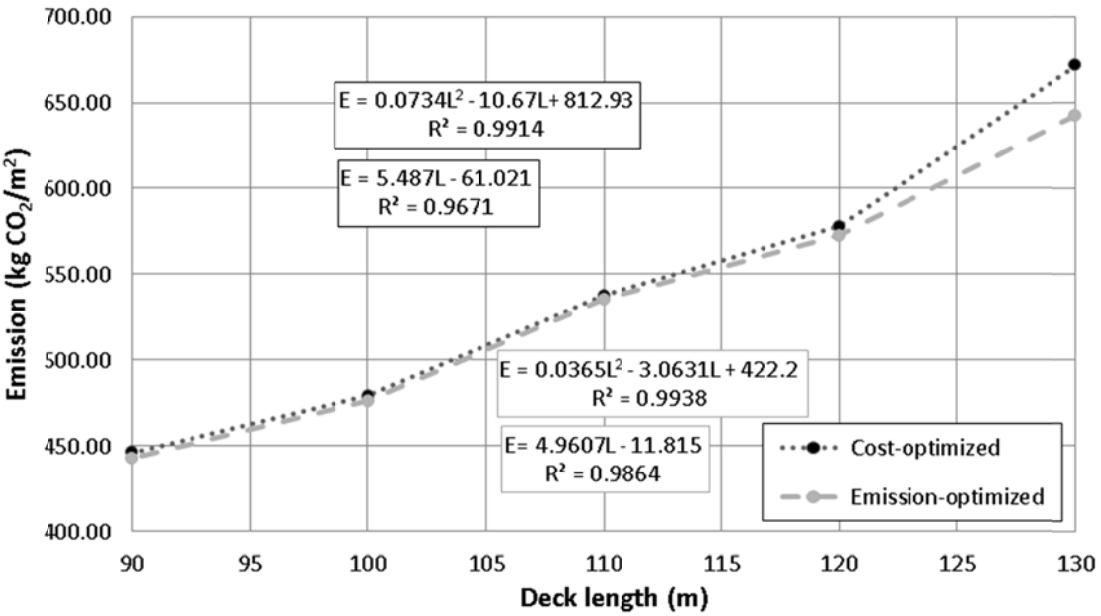


**Fig. 6.** Mean emission per $m^2$ of deck according to the deck length

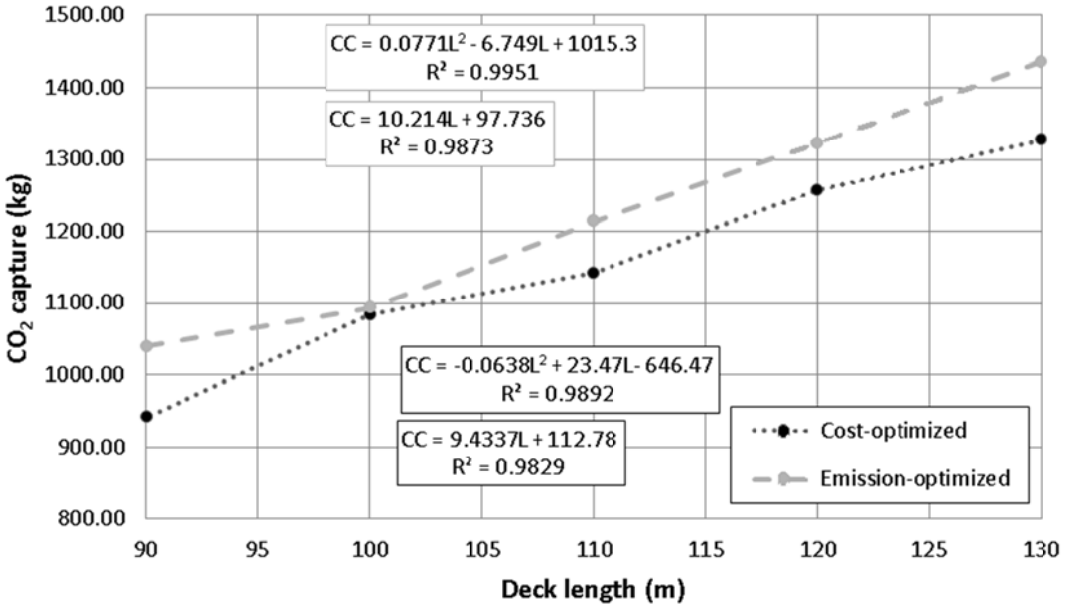


**Fig. 7.** Mean $CO_2$ capture according to the deck length

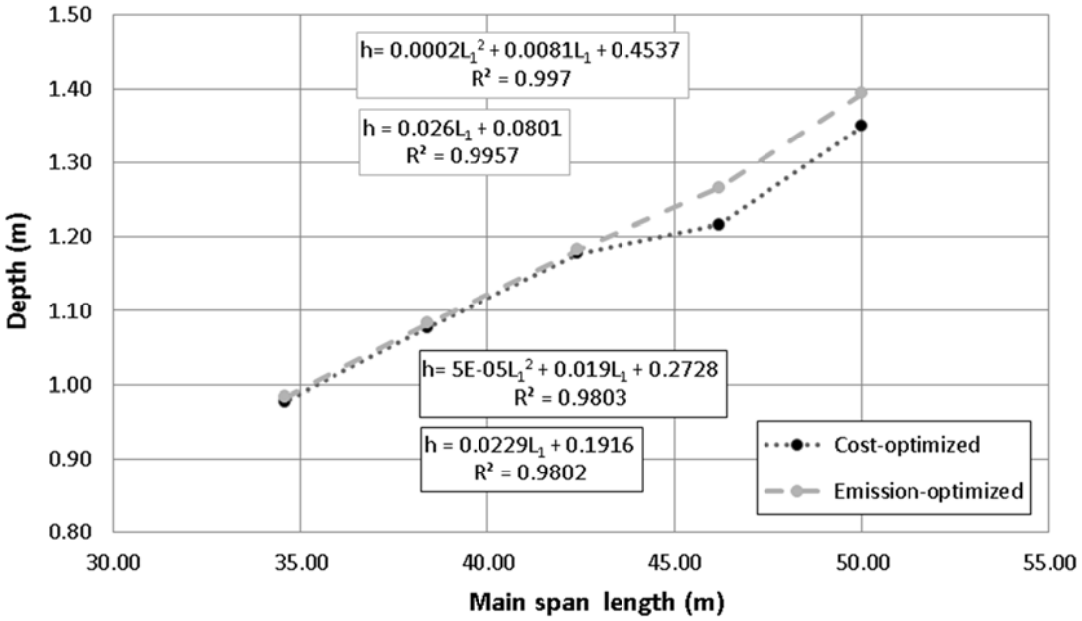


**Fig. 8.** Mean depth according to the span length

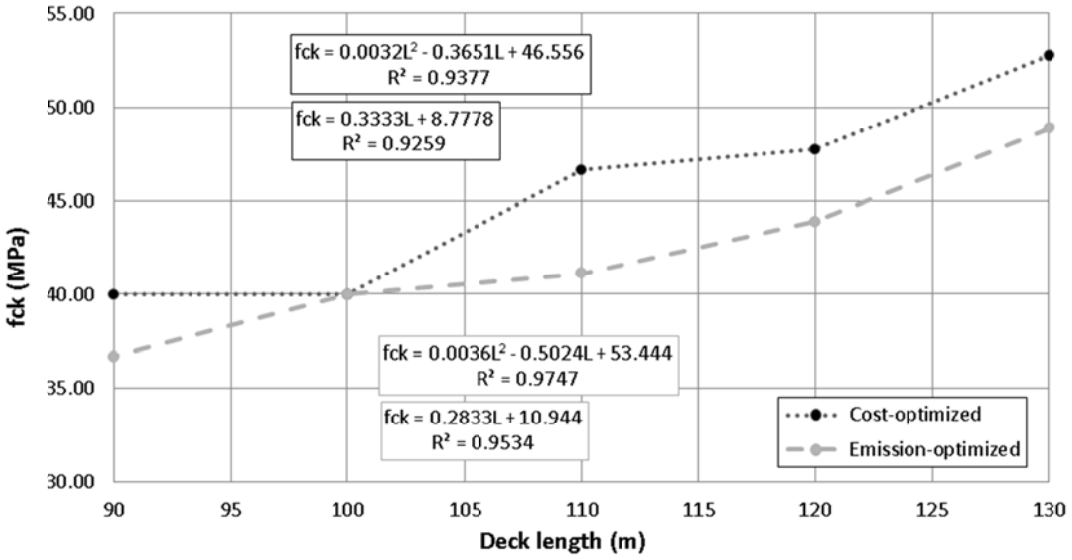


**Fig. 9.** Mean concrete strength according to the deck length

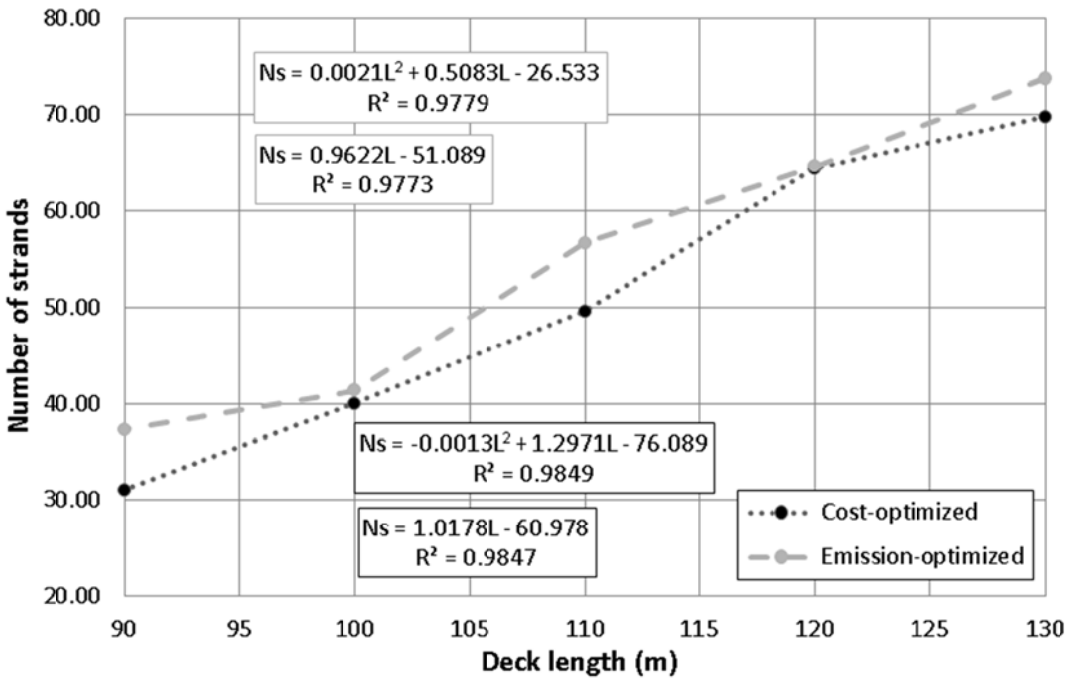


**Fig. 10.** Mean number of strands according to the deck length

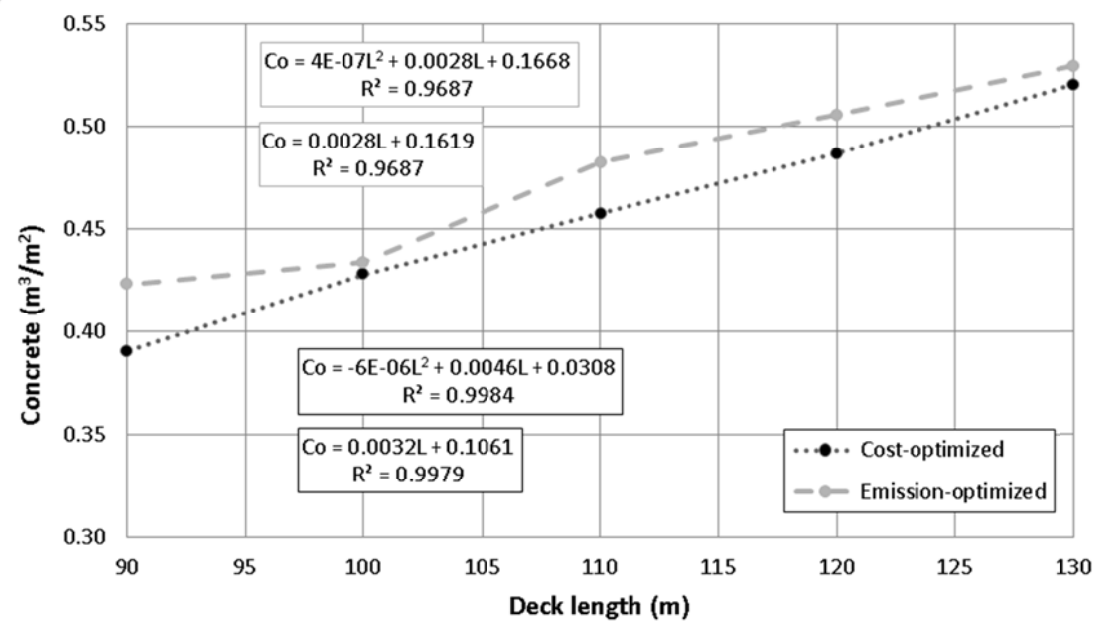


**Fig. 11.** Mean volume of concrete according to the deck length

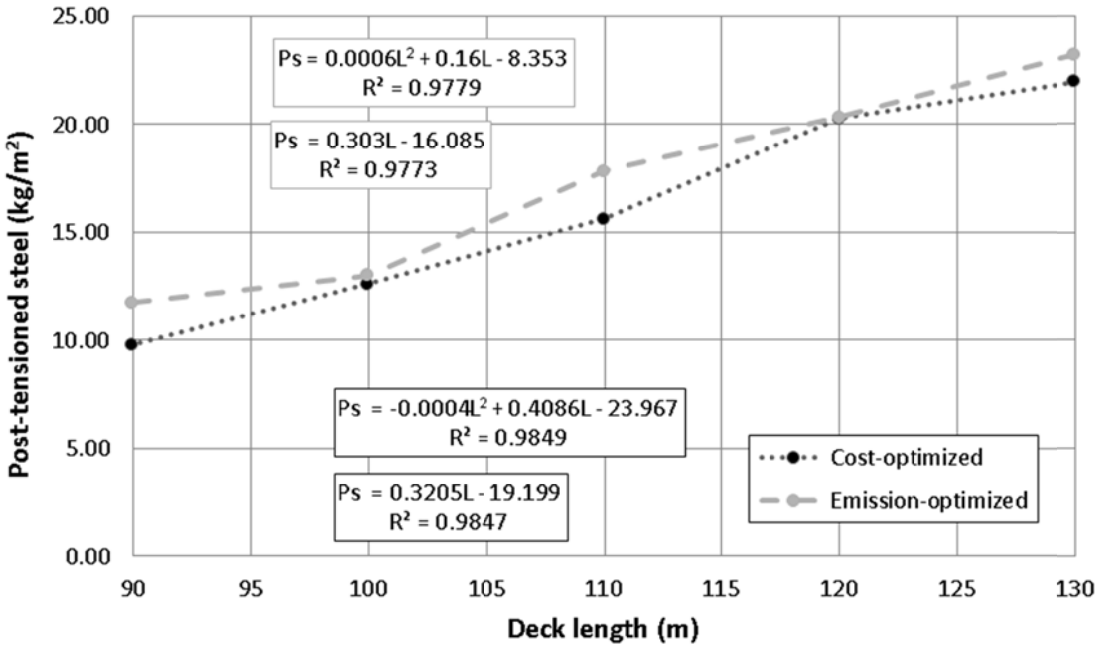


**Fig. 12.** Mean amount of post-tensioned steel according to the deck length

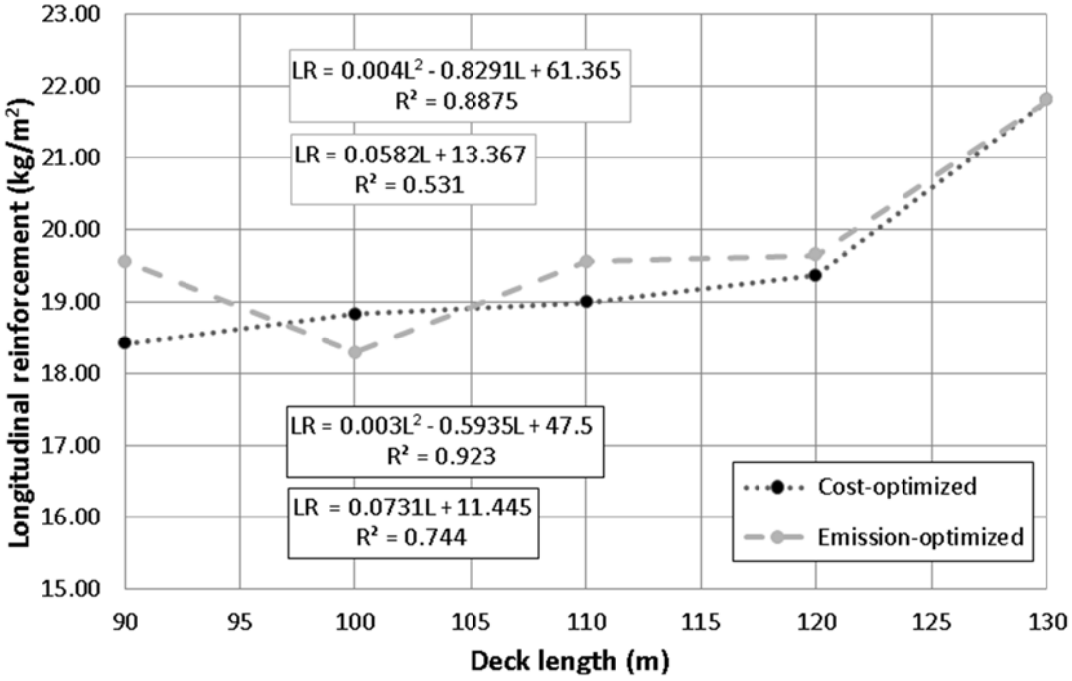


**Fig. 13.** Mean amount of longitudinal reinforcing steel according to the deck length

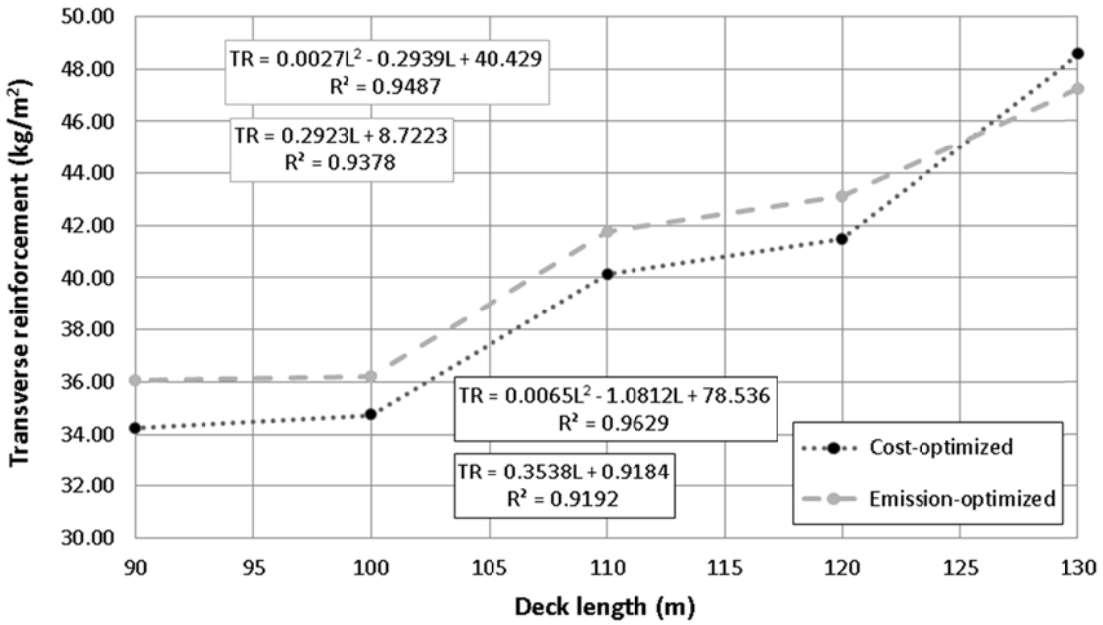


**Fig. 14.** Mean amount of transverse reinforcing steel according to the deck length